A Time-Domain Subspace Technique for Estimating Visual Evoked Potential Latencies

Mohd Zuki Yusoff and Nidal Kamel

Universiti Teknologi PETRONAS, Bandar Seri Iskandar, 31750 Tronoh, Perak, MALAYSIA

Summary
Estimating a visual evoked potential (VEP) from the human brain is challenging since its signal-to-noise ratio (SNR) is generally very low. An optimization and eigen-decomposition-based subspace approach has been investigated and tested to estimate the latencies of visual evoked potential (VEP) signals which are highly corrupted by spontaneous electro-encephalogram (EEG) waveforms that can be considered as colored noise. This scheme termed as the generalized subspace approach (GSA) depends on the generalized eigendecomposition of the covariance matrices of the VEP and the colored EEG noise. The subspace algorithm jointly transforms these two correlation matrices into diagonal matrices, which can then be segregated into signal subspace and noise subspace. Enhancement is performed by removing the noise subspace and estimating the clean VEP signal from the remaining signal subspace. Further, GSA has been compared with a third-order correlation (TOC) method, using both realistic simulation and real patient data gathered in a hospital. The simulation results produced by the GSA algorithm show more faithful reproduction of VEP waveforms, and a higher degree of consistencies in detecting the P100, P200, and P300 peaks. Additionally, the results of the real patient data confirm the superiority of GSA over TOC in estimating VEP's P100 latencies, which are used by clinicians to assess the conduction of electrical signals from the subjects' retinas to the visual cortex parts of their brains.

Keywords:
Visual evoked potentials, signal subspace, time-domain estimator, colored EEG noise, VEP latencies.

1. Introduction

A visual evoked potential (VEP) exists when a subject under study is shown a visual stimulation (e.g., a pattern reversal checkerboard). VEP latencies such as the P100's are used by clinicians to check the integrity of the visual pathways from the retina to the occipital cortex part of the brain [1]. The VEP is not immediately distinguishable from the brain recording because it is buried deep inside the ongoing electroencephalogram (EEG) noise, with a typical signal-to-noise ratio (SNR) of -5 to -10 dB [2, 3, 4, 5, 6]. The post-stimulation EEG which contaminates the VEP is highly colored and its correlation matrix cannot be directly obtained from the observed (corrupted) VEP; the pre-stimulation EEG which exists prior to the application of stimulation is the only sample that can be used to approximate the correlation matrix of the post-stimulation EEG.

Conventionally, ensemble averaging (EA) is used to extract the VEPs. For this, hundreds of trials need to be acquired and averaged out to really produce clean VEP estimates; this requires very long recording time that will certainly cause discomfort and fatigue to the subject under study; exhaustion will result in inconsistent formation of VEPs in terms of both amplitudes and latencies. Among the most recent "single-trial" approaches to detect VEPs is a third-order correlation (TOC) technique proposed by Gharieb and Cichocki [7]. This technique performs well in handling white and colored noise whose spectrum does not overlap with that of the desired signal. However, when the signal spectrum overlaps with the highly colored noise spectrum, the efficiency of the TOC-based technique is compromised.

The focus of this study is to correctly estimate VEP latencies, instead of VEP amplitudes. In hospitals, doctors are much more concerned about VEP latencies as opposed to VEP amplitudes; the latencies are used by clinicians to assess the visual pathway integrity of the patient under investigation. In general, an approach based on a signal subspace principle performs well in estimating the desired peak positions (i.e., latencies) of a given waveform.

The VEP extraction method presented here is inspired by work from a speech enhancement area, originally proposed by Ephraim and Van Trees [8]; the original work dealt primarily with white noise. The incorporation of universal optimization schemes in [8] makes them suitable for our single-trial estimation of VEPs. However, to deal with colored noise, we introduce generalized eigen-decomposition instead of normal eigen-decomposition operation in the underlying signal subspace estimator.

Manuscript received January 5, 2010
Manuscript revised January 20, 2010

The paper is organized as follows. The proposed generalized eigendecomposition technique is thoroughly discussed in section 2. Then, the TOC method is briefly outlined in section 3. Section 4 describes the results of VEP latency estimation in simulated and real environments. Section 5 concludes the paper.

To ensure common understanding and consistencies, all mathematical symbols, operators, notations and terminologies used are in compliance with the acceptable styles and conventions normally adopted worldwide. Lower case **boldface** characters will generally refer to vectors. Upper case **BOLDFACE** characters will generally refer to matrices. Vector or matrix transposition will be denoted using $(.)^T$, and $\Re^{MxM}$ denotes the real vector space of $M \times M$ dimensions.

2. Model Development

2.1 VEP Model

It is assumed that a VEP is actually a "known" waveform which can be artificially produced. The created VEP will then be added to much higher power "colored noise" that represents EEG and other background noise. The resultant waveform will be treated as a composite signal that needs to be processed and extracted using the developed technique to get back the desired VEP. Thus, the following model is defined.

$$\boldsymbol{y} = \boldsymbol{x} + \boldsymbol{n} \tag{1}$$

where, $\boldsymbol{y}$ is the M-dimensional vector of the corrupted (noisy) VEP signal; $\boldsymbol{x}$ is the M-dimensional vector of the original (clean) VEP signal; $\boldsymbol{n}$ is the M-dimensional vector of the additive EEG noise which is assumed to be uncorrelated with $\boldsymbol{x}$. Further, $\boldsymbol{H}$ is defined as the M x M-dimensional matrix of the VEP time-domain constrained linear estimator.

Next, $\hat{\boldsymbol{x}}$ is defined as the M-dimensional vector of the estimated VEP signal. The estimated VEP signal $\hat{\boldsymbol{x}}$ is related to $\boldsymbol{H}$ and $\boldsymbol{y}$ in the following way [8]:

$$\hat{\boldsymbol{x}} = \boldsymbol{H}.\boldsymbol{y} \tag{2}$$

The estimated VEP signal $\hat{\boldsymbol{x}}$ will never be exactly equal to the original VEP signal $\boldsymbol{x}$; the error signal $\boldsymbol{\varepsilon}$ defined by [8] is written as:

$$\begin{aligned} \boldsymbol{\varepsilon} &= \hat{\boldsymbol{x}} - \boldsymbol{x} = \boldsymbol{H}\boldsymbol{y} - \boldsymbol{x} = (\boldsymbol{H} - \boldsymbol{I})\boldsymbol{x} + \boldsymbol{H}\boldsymbol{n} \\ &= \boldsymbol{\varepsilon}_x + \boldsymbol{\varepsilon}_n \quad \text{where } \boldsymbol{\varepsilon}_x = (\boldsymbol{H} - \boldsymbol{I})\boldsymbol{x}, \quad \boldsymbol{\varepsilon}_n = \boldsymbol{H}\boldsymbol{n} \end{aligned} \tag{3}$$

The $\boldsymbol{\varepsilon}_x$ represents the VEP distortion and $\boldsymbol{\varepsilon}_n$ represents the residual noise. If the VEP signal correlation matrix $\boldsymbol{R}_x$ is known, then the energies of the signal distortion can be written as

$$\bar{\boldsymbol{\varepsilon}}_{\boldsymbol{x}}^2 = \mathrm{tr}\left(E\left\{\boldsymbol{\varepsilon}_x \boldsymbol{\varepsilon}_x^T\right\}\right) = \mathrm{tr}\left((\boldsymbol{H} - \boldsymbol{I})\boldsymbol{R}_x(\boldsymbol{H} - \boldsymbol{I})^T\right) \tag{4}$$

Similarly, if the EEG noise correlation matrix $\boldsymbol{R}_n$ is known, the energies of the residual noise can be expressed as

$$\bar{\boldsymbol{\varepsilon}}_n^2 = \mathrm{tr}\left(E\left\{\boldsymbol{\varepsilon}_n \boldsymbol{\varepsilon}_n^T\right\}\right) = \mathrm{tr}\left(\boldsymbol{H}\boldsymbol{R}_n\boldsymbol{H}^T\right) \tag{5}$$

Both energies in Eqs. (4) and (5) lead to the total residual energies given as

$$\bar{\boldsymbol{\varepsilon}}^2 = \bar{\boldsymbol{\varepsilon}}_x^2 + \bar{\boldsymbol{\varepsilon}}_n^2 \tag{6}$$

The EEG noise correlation matrix $\boldsymbol{R}_n$ can be obtained from the pre-stimulation EEG samples, during which the VEP signals are absent. If the VEP and EEG noise are independent, the following relationships can be established:

$$\boldsymbol{R}_y = \boldsymbol{R}_x + \boldsymbol{R}_n \tag{7}$$

where, $\boldsymbol{R}_y$ is the correlation matrix of the corrupted VEP. Using Eq. (7), we can calculate $\boldsymbol{R}_x$ by subtracting $\boldsymbol{R}_n$ from $\boldsymbol{R}_y$.

2.2 Estimator Optimization

An optimal time-domain constrained linear estimator $\boldsymbol{H}$ that minimizes the VEP signal distortion and maintains the residual noise within a permissible level, is mathematically formulated by [8] as

$$\boldsymbol{H}_{opt} = \min_{\boldsymbol{H}} \bar{\boldsymbol{\varepsilon}}_x^2 \ \text{ subject to} : \bar{\boldsymbol{\varepsilon}}_n^2 \le M\sigma^2 \tag{8}$$

where M is the dimension of the noisy vector space and σ^2 is a positive constant noise threshold level. The σ^2 in Eq. (8) dictates the amount of the residual noise allowed to remain in the linear estimator. Next, the Lagrangian function in association with the "Kuhn-Tucker necessary conditions for constrained minimization" [8] are applied to Eq. (8) to obtain $\boldsymbol{H}_{opt}$. The formed Lagrangian function can be expressed as

$$\boldsymbol{L}(\boldsymbol{H}, \mu) = \bar{\boldsymbol{\varepsilon}}_x^2 + \mu(\bar{\boldsymbol{\varepsilon}}_n^2 - M\sigma^2) \tag{9}$$

where μ is the Lagrange multiplier. It follows that the filter matrix $\boldsymbol{H}$ is a stationary feasible point if it satisfies the
following gradient equation $\nabla_H \boldsymbol{L}(\boldsymbol{H}, \mu) = 0$:

$$\frac{\partial \boldsymbol{L}(\boldsymbol{H}, \mu)}{\partial \boldsymbol{H}} = \frac{\partial}{\partial \boldsymbol{H}}[\bar{\boldsymbol{\varepsilon}}_x^2 + \mu(\bar{\boldsymbol{\varepsilon}}_n^2 - M\sigma^2)] = 0 \tag{10}$$

Subsequently, the gradient equation in Eq. (10) can be solved to yield $\boldsymbol{H}$.

$$\begin{aligned} &\frac{\partial}{\partial \boldsymbol{H}}[\mathrm{tr}\left((\boldsymbol{H}-\boldsymbol{I})\boldsymbol{R}_x(\boldsymbol{H}-\boldsymbol{I})^T\right)]+\frac{\partial}{\partial \boldsymbol{H}}[\mu \mathrm{tr}\left(\boldsymbol{H}\boldsymbol{R}_n\boldsymbol{H}^T\right)]=0 \\ &2(\boldsymbol{H}-\boldsymbol{I})\boldsymbol{R}_x+2\mu\boldsymbol{H}\boldsymbol{R}_n-0=0 \\ &\Rightarrow \boldsymbol{H}=\boldsymbol{R}_x(\boldsymbol{R}_x+\mu\boldsymbol{R}_n)^{-1} \end{aligned} \quad (11)$$

The filter matrix $\boldsymbol{H}$ stated in Eq. (11) functions as a fixed filter, which performs well to estimate the VEP at a relatively high SNR. As the SNR degrades, it is desirable if $\boldsymbol{H}$ can be adjusted and manipulated accordingly to minimize the noise residues while keeping the signal distortion at an acceptable level. A difficulty arises since lowering noise energies means increasing the distortion energies, and vice versa. Therefore, a proper balance needs to be determined so that the noise residues can be reasonably reduced without introducing significant distortion to the processed signal. The excessive amount of the residual noise prohibits the discrimination between the desired VEP peak (e.g., the P100) and the noise peaks themselves, even if the desired signal is successfully extracted. On the other hand, the excessive distortion means the desired VEP peak may have shifted either to the left or right of its original position, resulting in an inaccurate measurement of the VEP latency.

Equation (11) can be simplified by attempting eigenvalue decomposition operation on $\boldsymbol{R}_x$ and $\boldsymbol{R}_n$. Theoretically, the decomposition process separates the noisy VEP space into the signal subspace and noise subspace; the signal subspace segment is preserved for further manipulations, while the noise portion is totally discarded. The challenge is to actually be able to fully and simultaneously diagonalize both $\boldsymbol{R}_x$ and $\boldsymbol{R}_n$ to achieve absolute decorrelation, before any rank reduction in the signal subspace component can be performed.

2.3 Karhunen-Loeve Transform

The Karhunen-Loeve Transform (KLT) is a unitary linear transform widely applied in signal processing areas. The KLT scheme exploits the statistical properties of a discrete-time stochastic process; KLT optimally decorrelates the process by means of diagonalizing its correlation matrix.

Theorem 1 (Karhunen-Loeve Transform [9]). Let $\boldsymbol{R}_a$ be the MxM symmetric correlation matrix of a discrete-time stochastic process $a(n)$. Further, let $\boldsymbol{V}_a$ and $\boldsymbol{D}_a$ be the corresponding MxM unitary eigenvector and eigenvalue matrices of $\boldsymbol{R}_a$. Then KLT is defined as the unitary transform of the following form:

$$\boldsymbol{R}_a=\boldsymbol{V}_a\boldsymbol{D}_a\boldsymbol{V}_a^{-1}=\boldsymbol{V}_a\boldsymbol{D}_a\boldsymbol{V}_a^T,\ \boldsymbol{V}_a^{-1}=\boldsymbol{V}_a^T \text{ for unitary } \boldsymbol{V}_a \quad (12)$$

The relationships among various parameters established in Eq. (12) can be achieved by taking eigendecomposition on $\boldsymbol{R}_a$. It follows that Eq. (12) above can be rearranged and simplified accordingly to compute the diagonal eigenvalue $\boldsymbol{D}_a = \mathrm{diag}\,[d_1, d_2, ..., d_M]$; that is

$$\boldsymbol{D}_a=\boldsymbol{V}_a^{-1}\boldsymbol{R}_a\boldsymbol{V}_a^{-T}=\boldsymbol{V}_a^T\boldsymbol{R}_a\boldsymbol{V}_a,\ \boldsymbol{V}_a^{-T}=\boldsymbol{V}_a \text{ for unitary } \boldsymbol{V}_a \quad (13)$$

Equation (13) reveals that $\boldsymbol{R}_a$ is transformed by the $\boldsymbol{V}_a^T$ (i.e., KLT matrix) and $\boldsymbol{V}_a$ (i.e., inverse KLT) terms into the diagonal matrix $\boldsymbol{D}_a$, resulting in the optimal decorrelation of the stochastic process.

Proof: The KLT and IKLT concept involving a column vector $\boldsymbol{a}$ and its symmetric correlation matrix $\boldsymbol{R}_a$, is represented by a block diagram shown in Fig. 1 below.

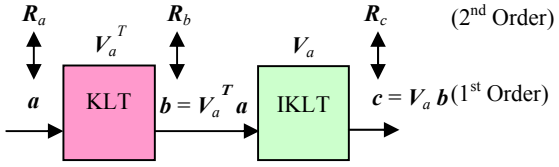

Fig. 1 KLT and IKLT schemes involving an original vector $\boldsymbol{a}$ and its unitary eigenvector $\boldsymbol{V}_a$.

With reference to Fig. 1, let $\boldsymbol{b}$ represent a column vector after the KLT of $\boldsymbol{a}$, and let $\boldsymbol{c}$ represent a column vector after the IKLT block. The transformation of $\boldsymbol{a}$ into $\boldsymbol{b}$ is achieved using the KLT matrix $\boldsymbol{V}_a^T$:

$$\boldsymbol{b}=\boldsymbol{V}_a^{-1}\boldsymbol{a}=\boldsymbol{V}_a^T\boldsymbol{a} \quad (14)$$

To obtain decorrelation, the correlation matrix of $\boldsymbol{b}$ is computed as the expectation of the outer product of $\boldsymbol{b}$ by itself, written as

$$\boldsymbol{R}_b=E\{\boldsymbol{b}\boldsymbol{b}^T\}=E\{\boldsymbol{V}_a^T\boldsymbol{a}(\boldsymbol{V}_a^T\boldsymbol{a})^T\}=\boldsymbol{V}_a^T\boldsymbol{R}_a\boldsymbol{V}_a=\boldsymbol{D}_a \quad (15)$$

The matrix $\boldsymbol{R}_a$ is linearly transformed into $\boldsymbol{R}_b$ by the $\boldsymbol{V}_a^T\boldsymbol{R}_a\boldsymbol{V}_a$ term; the correlation matrix $\boldsymbol{R}_b$ of $\boldsymbol{b}$ is actually the eigenvalue matrix $\boldsymbol{D}_a$ of $\boldsymbol{R}_a$. Since $\boldsymbol{R}_b$ is fully diagonal, it can be concluded that the cross-correlation has been removed. In order to return to the original space (with a reduced rank) prior to the transform in the KLT domain, the inverse transform using the IKLT matrix $\boldsymbol{V}_a$ needs to be performed on $\boldsymbol{b}$; that is,

$$\boldsymbol{c}=\boldsymbol{V}_a\boldsymbol{b}=\boldsymbol{V}_a\boldsymbol{V}_a^T\boldsymbol{a}=\boldsymbol{a} \quad (16)$$

From Eq. (16), it is clear that the original vector $\boldsymbol{a}$ has been recovered. Furthermore, the correlation matrix of $\boldsymbol{c}$ is computed as the expectation of the outer product of $\boldsymbol{c}$ by itself, written as

$$\begin{aligned} \boldsymbol{R}_c &= E\{\boldsymbol{c}\boldsymbol{c}^T\} = E\{\boldsymbol{V}_a\boldsymbol{b}(\boldsymbol{V}_a\boldsymbol{b})^T\} = \boldsymbol{V}_a\boldsymbol{R}_b\boldsymbol{V}_a^T \\ &= \boldsymbol{V}_a\boldsymbol{V}_a^T\boldsymbol{R}_a\boldsymbol{V}_a\boldsymbol{V}_a^T = \boldsymbol{R}_a \quad \text{where } \boldsymbol{R}_b = \boldsymbol{V}_a^T\boldsymbol{R}_a\boldsymbol{V}_a \end{aligned} \tag{17}$$

From Eq. (17), it is clear that the correlation matrix $\boldsymbol{R}_a$ has been recovered by taking the linear inverse transform of $\boldsymbol{R}_b$ denoted by the $\boldsymbol{V}_a\boldsymbol{R}_b\boldsymbol{V}_a^T$ term. Alternatively, the KLT expansion is termed as a *subspace estimator* when some of the decomposed orthogonal components are truncated to reject noise. The truncation means some eigenvalues and corresponding eigenvectors carrying unwanted elements are removed; only the components deemed to be significant are retained in the process. The reduced matrix is then reconstructed to estimate the required signal. In brief, the decomposition and decorrelation of a noisy observation can be performed using eigenvalue decomposition (EVD).

2.4 Non-Unitary Linear Transform

The symmetric basis matrix $\boldsymbol{R}_a$ discussed in the previous subsection can be the result of a linear summation between two symmetric matrices such as $\boldsymbol{R}_x$ and $\boldsymbol{R}_n$. We have also shown that KLT and IKLT can always be applied on a basis matrix which is symmetric. However, if the chosen basis matrix $\boldsymbol{R}_d$ is not symmetric (e.g., $\boldsymbol{R}_d = \boldsymbol{R}_n^{-1}\boldsymbol{R}_x$, given that individual $\boldsymbol{R}_x$ or $\boldsymbol{R}_n$ is symmetric), then the EVD of $\boldsymbol{R}_d$ results in a non-unitary eigenvector matrix $\boldsymbol{V}_d$. In this case, the KLT concept cannot be applied; $\boldsymbol{V}_d^T$ and $\boldsymbol{V}_d$ are no longer the KLT and IKLT matrices.

For the non-unitary eigenvector matrix $\boldsymbol{V}_d$ stated above, the proper matrices for the linear forward (non-KLT) and linear inverse (non-IKLT) transform blocks are $\boldsymbol{V}_d^T$ and $\boldsymbol{V}_d^{-T}$, respectively.

Proof: A transformation of column vector $\boldsymbol{d}$ and its non-symmetric correlation matrix $\boldsymbol{R}_d$ is represented by a block diagram shown in Fig. 2 below.

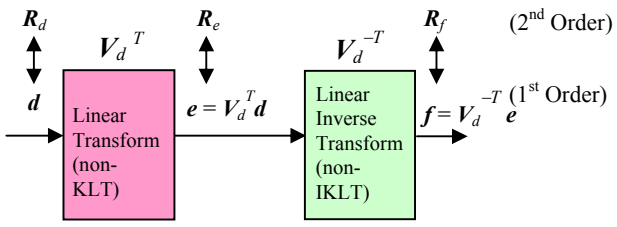

Fig. 2 Non-KLT and non-IKLT transforms involving a non-symmetric basis matrix $\boldsymbol{d}$ and its corresponding non-unitary eigenvector matrix $\boldsymbol{V}_d$.

With reference to Fig. 2, let $\boldsymbol{e}$ represent a column vector after the linear forward transform of $\boldsymbol{d}$, and let $\boldsymbol{f}$ represent a column vector after the linear inverse transform block. The transformation of $\boldsymbol{d}$ into $\boldsymbol{e}$ is achieved using the linear transform matrix $\boldsymbol{V}_d^T$.

$$\boldsymbol{e} = \boldsymbol{V}_d^T\boldsymbol{d} \tag{18}$$

The correlation matrix of $\boldsymbol{e}$ is computed as the expectation of the outer product of $\boldsymbol{e}$ by itself, written as

$$\boldsymbol{R}_e = E\{\boldsymbol{e}\boldsymbol{e}^T\} = E\{\boldsymbol{V}_d^T\boldsymbol{d}(\boldsymbol{V}_d^T\boldsymbol{d})^T\} = \boldsymbol{T}_d \tag{19}$$

The matrix $\boldsymbol{R}_d$ is linearly transformed into $\boldsymbol{R}_e$ by the $\boldsymbol{V}_d^T\boldsymbol{R}_d\boldsymbol{V}_d$ term; this time, the diagonal $\boldsymbol{R}_e$ is equal to the eigenvalue $\boldsymbol{T}_d$ of $\boldsymbol{R}_d$—this is a clear case of decorrelation. Further, the inverse transform using $\boldsymbol{V}_d^{-T}$ is performed on $\boldsymbol{e}$ to get back $\boldsymbol{d}$.

$$\boldsymbol{f} = \boldsymbol{V}_d^{-T}\boldsymbol{e} = \boldsymbol{d} \tag{20}$$

The correlation matrix of $\boldsymbol{f}$ is given as

$$\boldsymbol{R}_f = E\{\boldsymbol{f}\boldsymbol{f}^T\} = E\{\boldsymbol{V}_d^{-T}\boldsymbol{e}(\boldsymbol{V}_d^{-T}\boldsymbol{e})^T\} = \boldsymbol{R}_d \tag{21}$$

With reference to Eq. (21), $\boldsymbol{R}_f$ is equal to $\boldsymbol{R}_d$; this implies that the inverse transform restructures $\boldsymbol{R}_e$ back into $\boldsymbol{R}_d$.

In short, a non-KLT linear transform and a non-IKLT linear inverse transform are still possible using non-unitary eigenvectors – providing that great care is taken in the selection of a basis matrix, the formation of transform and inverse transform matrices from the resulting non-unitary eigenvectors, and the choice of a matrix or matrices to be decorrelated.

Next, the forward non-KLT expansion to decompose and decorrelate a noisy observation can be performed using EVD. Later, manipulations can be performed on the decorrelated components. For example, certain decomposed orthogonal components considered as belonging to the dominant noise subspace may be omitted. The elimination means the dimensions of the eigenvalues and their corresponding eigenvectors are reduced; the matrices with the reduced dimensions should then represent the dominant signal subspace which consists of significant components. Eventually, the rank-reduced matrix is reconstructed to estimate the required VEP signal.

2.5 Generic Concepts of a Subspace Method

With reference to Eq. (11), eigenvalue decomposition is to be performed on $\boldsymbol{R}_x$ and $\boldsymbol{R}_n$. By assuming that $\boldsymbol{R}_x = \boldsymbol{U}\boldsymbol{\Delta}_x\boldsymbol{U}^T$ and $\boldsymbol{R}_n = \boldsymbol{U}\boldsymbol{\Delta}_n\boldsymbol{U}^T$ exist (as in the case of white noise), we rewrite Eq. (11) as

$$\boldsymbol{H}_{opt} = \boldsymbol{U}\boldsymbol{\Delta}_x(\boldsymbol{\Delta}_x + \mu\boldsymbol{\Delta}_n)^{-1}\boldsymbol{U}^T \quad (22)$$

where, $\boldsymbol{H}_{opt}$ denotes an optimal estimator; $\boldsymbol{U}$ is the unitary eigenvector matrix produced from a symmetric basis matrix $\boldsymbol{\Sigma}$ which is to be computed from the proper combinations of $\boldsymbol{R}_x$ and $\boldsymbol{R}_n$ terms; $\boldsymbol{\Delta}_x$ is the diagonal eigenvalue matrix of $\boldsymbol{R}_x$; $\boldsymbol{\Delta}_n$ is the diagonal eigenvalue matrix of $\boldsymbol{R}_n$; μ is the Lagrange multiplier which has to be set to a proper value. The higher value of μ eliminates more noise residues at the expense of higher distortion in the recovered VEP.

Theoretically, the linear estimator in Eq. (22) functions optimally if the unitary eigenvector matrix $\boldsymbol{U}$ derived from the eigendecomposition of $\boldsymbol{\Sigma}$ is able to simultaneously diagonalize both $\boldsymbol{R}_x$ and $\boldsymbol{R}_n$. For white noise cases, this simultaneous diagonalization can be perfectly achieved by treating $\boldsymbol{\Sigma} = \boldsymbol{R}_y = \boldsymbol{R}_x + \boldsymbol{R}_n$; $\boldsymbol{U}$ diagonalizes not only $\boldsymbol{R}_y$, but also $\boldsymbol{R}_x$ and $\boldsymbol{R}_n$. However for colored noise, $\boldsymbol{\Delta}_x$ and $\boldsymbol{\Delta}_n$ in Eq. (22) are no longer diagonal if they are equated with $\boldsymbol{U}^T\boldsymbol{R}_x\boldsymbol{U}$ and $\boldsymbol{U}^T\boldsymbol{R}_n\boldsymbol{U}$, respectively. For colored noise scenarios, if $\boldsymbol{U}$ is the eigenvector matrix of $\boldsymbol{R}_y$, it diagonalizes only $\boldsymbol{R}_y$ and not $\boldsymbol{R}_x$ or $\boldsymbol{R}_n$. Moreover, for colored noise sources such as EEGs, full diagonalization can no longer be obtained if further manipulation on Eq. (22) is not performed.

Mathematically, the full diagonalization of their eigenvalues can be obtained if and only if $\boldsymbol{R}_x$ and $\boldsymbol{R}_n$ multiplication is commutative (i.e., $\boldsymbol{R}_x\boldsymbol{R}_n = \boldsymbol{R}_n\boldsymbol{R}_x$). In reality, complete diagonalization (i.e., without any pre-whitening mechanism) is not possible since their multiplication is non-commutative. To reduce the colored noise case to the estimator in [8], we may prewhiten the noise by using inverse filtering or look for transformation that simultaneously diagonalizes $\boldsymbol{R}_x$ and $\boldsymbol{R}_n$ as

$$\boldsymbol{E}^T\boldsymbol{R}_x\boldsymbol{E} = \boldsymbol{F}_x = \boldsymbol{F} \quad (23)$$

$$\boldsymbol{E}^T\boldsymbol{R}_n\boldsymbol{E} = \boldsymbol{F}_n = \boldsymbol{I} \quad (24)$$

where $\boldsymbol{E}$ and $\boldsymbol{F}$ are the pertinent eigenvector and eigenvalue matrices of a non-symmetric basis matrix $\boldsymbol{\Psi} = \boldsymbol{R}_n^{-1}\boldsymbol{R}_x$. We obtain the eigendecomposition of the matrix $\boldsymbol{\Psi} = \boldsymbol{R}_n^{-1}\boldsymbol{R}_x$ as

$$\boldsymbol{R}_n^{-1}\boldsymbol{R}_x\boldsymbol{V} = \boldsymbol{E}\boldsymbol{F} \quad (25)$$

after relating Eq. (23) to Eq. (24).

2.6 Generalized Subspace Approach

An explicit pre-whitening scheme shown in Eq. (25) inverses a matrix; the inversion introduces a drawback and is critical from a numerical point of view when the matrix is ill-conditioned. Alternatively, the explicit pre-whitening approach can be replaced by implicit pre-whitening which can be performed by the generalized eigen-decomposition [10] of the matrix pair ($\boldsymbol{R}_x$, $\boldsymbol{R}_n$), as follows:

$$\boldsymbol{R}_x\boldsymbol{V} = \boldsymbol{R}_n\boldsymbol{V}\boldsymbol{\Lambda} \quad (26)$$

where $\boldsymbol{\Lambda}$ is a diagonal $M \times M$ matrix that contains the generalized eigenvalues and $\boldsymbol{V}$ contains the generalized eigenvectors. In fact, we replaced the unitary eigenvectors $\boldsymbol{U}$ in Eq. (22) with the generalized eigenvectors $\boldsymbol{V}$; this time, $\boldsymbol{V}$ in Eq. (26) is a non-unitary eigenvector matrix which transforms jointly both $\boldsymbol{R}_x$ and $\boldsymbol{R}_n$ to the following diagonal matrices.

$$\boldsymbol{V}^T\boldsymbol{R}_x\boldsymbol{V} = \boldsymbol{\Lambda}_x = \boldsymbol{\Lambda} \quad (27)$$

$$\boldsymbol{V}^T\boldsymbol{R}_n\boldsymbol{V} = \boldsymbol{\Lambda}_n = \boldsymbol{I} \quad (28)$$

An optimal estimator $\boldsymbol{H}_{GEIG}$ based on the generalized eigendecomposition of ($\boldsymbol{R}_x$, $\boldsymbol{R}_n$) can then be obtained by applying Eqs. (26), (27) and (28) to Eq. (11):

$$\begin{aligned}\boldsymbol{H}_{GEIG} &= \boldsymbol{R}_n\boldsymbol{V}\boldsymbol{\Lambda}\left(\boldsymbol{\Lambda} + \mu\boldsymbol{I}\right)^{-1}\boldsymbol{V}^T \\ &= \boldsymbol{V}^{-T}\boldsymbol{\Lambda}\left(\boldsymbol{\Lambda} + \mu\boldsymbol{I}\right)^{-1}\boldsymbol{V}^T\end{aligned} \quad (29)$$

Equation (29) can now be used to replace Eq. (22) to estimate a signal which is corrupted either by white or colored noise. Based on Eqs. (2) and (29), the estimated VEP is then calculated as

$$\begin{aligned}\hat{\boldsymbol{x}} &= \boldsymbol{H}_{GEIG} \bullet \boldsymbol{y} = \boldsymbol{R}_n\boldsymbol{V}\boldsymbol{G}\boldsymbol{V}^T \bullet \boldsymbol{y} \\ &= \boldsymbol{V}^{-T}\boldsymbol{G}\boldsymbol{V}^T \bullet \boldsymbol{y} \qquad \text{where } \boldsymbol{G} = \boldsymbol{\Lambda}(\boldsymbol{\Lambda} + \mu\boldsymbol{I})^{-1}\end{aligned} \quad (30)$$

The corrupted VEP signal $\boldsymbol{y}$ in Eq. (30) is decorrelated by the KLT matrix $\boldsymbol{V}^T$. Then, the transformed signal is modified and enhanced by a signal subspace gain matrix $\boldsymbol{G}$. Next, the modified signal is retransformed back into the original state (at a reduced rank) by the inverse KLT matrix $\boldsymbol{V}^{-T}$ to approximate the desired VEP signal.

2.7 Algorithm Implementation

The proposed approach can be formulated in the following ten steps:

Step 1. Compute the correlation matrix of the brain background colored noise $\boldsymbol{R}_n$, using the pre-stimulation EEG sample.

Step 2. Compute the noisy VEP correlation matrix $\boldsymbol{R}_y$, using the observed (corrupted) sample.

Step 3. Estimate the correlation matrix of the noiseless VEP sample as $\boldsymbol{R}_x = \boldsymbol{R}_y - \boldsymbol{R}_n$.

Step 4. Perform the generalized eigendecomposition on $\boldsymbol{R}_x$ and $\boldsymbol{R}_n$ using Eq. (26). Extract the eigenvector matrix $\boldsymbol{V}$ and eigenvalue matrix $\boldsymbol{\Lambda}$ from the computation.

Step 5. Assuming that the generalized eigenvalues of $\boldsymbol{\Lambda}$ are ordered as $\lambda_1 \geq \lambda_2 \geq \ \ldots \ \geq \lambda_M$, estimate the dimension of the VEP signal subspace as follows:

$$d = \arg\{ \max_{1 \leq k \leq M} \ \lambda_k > 0 \} \qquad (31)$$

Step 6. Form a diagonal matrix, $\boldsymbol{\Lambda}_M$, from the largest M diagonal values of $\boldsymbol{\Lambda}$.

Step 7. Form a matrix $\boldsymbol{V}_M$ using eigenvectors of $\boldsymbol{V}$ that correspond to the largest M eigenvalues.

Step 8. Choose a proper value for μ as a compromise between signal distortion and noise residues. Experimentally, $\mu = 2$ was found to be ideal in reducing the EEG noise to a certain level, while minimizing the VEP signal distortion at the same time.

Step 9. Compute the optimal linear estimator using Eq. (29).

Step 10. Estimate the desired VEP signal using Eq. (30).

3. Third Order Correlation Approach

A third-order correlation (TOC)-based filtering approach has been proposed by Gharieb and Cichocki [7] to extract VEPs from noisy observations. Reference [7] noted that higher order statistics, also known as cumulants, preserves the signal structure of a noise free signal. Further, cumulants exhibit high tolerance to white or colored Gaussian noise and other symmetrically distributed white or colored non-Gaussian noise [7].

The philosophy behind the TOC is to feed the noisy observations through a finite impulse response (FIR) filter and obtain a good estimate of the VEP at the filter's output. For this purpose, the TOCs are utilized to compute the impulse response of the filter; the bandpass of the FIR filter is to be matched with the shape of the clean VEP alone. However, since the actual VEP signal is not *a priori* known, [7] proposed the impulse response of the FIR to be proportional with "an estimate of the selected TOCs of the noisy signal" .

For finite data length, the one dimensional TOC slice of the noisy signal $\boldsymbol{y}(n)$, is given by the following equation:

$$\hat{\boldsymbol{c}}_y(\tau) = \frac{1}{N} \sum_{n=0}^{N_1} \boldsymbol{y}^*(n)\, \boldsymbol{y}(n+\tau)\, \boldsymbol{y}(n+\tau_0) \qquad (32)$$

in which N is the number of available data points and $N_1 = \min[N-1,\ N-1-\tau,\ N-1-\tau_0]$, $\tau \geq 0$, τ_0 is a positive constant. Given a filter order P, the impulse response $\boldsymbol{h}(m)$, can be estimated as

$$\boldsymbol{h}(m) = \begin{cases} \hat{c}_y(P-m), & m = 0,\ 1,\ \cdots,\ P \\ \hat{c}_y(m-P), & m = P+1,\ P+2,\ \cdots,\ 2P \end{cases} \qquad (33)$$

Finally, the enhanced signal $\hat{\boldsymbol{x}}$ which is available at the output of the FIR filter is given by

$$\hat{\boldsymbol{x}}(n) = \sum_{m=0}^{2P} \boldsymbol{h}(m)\, \boldsymbol{y}(n-m) \qquad (34)$$

4. Experiments, Results and Discussions

4.1 Simulated Data

In this subsection, the performances of the GSA and TOC in estimating the P100, P200, and P300 are tested in statistical forms using artificially generated VEP signals corrupted with colored noise at different SNR values.

Artificial VEP and EEG waveforms are generated and added to each other in order to create a noisy VEP. The clean VEP $\boldsymbol{x}(k) \in \Re^M$, is generated by superimposing J Gaussian functions [11], each of which having a different amplitude (A), variance (σ^2) and mean (μ) as given by the following equation:

$$\boldsymbol{x}(k) = \left[\sum_{n=1}^{J} \boldsymbol{g}_n(k) \right]^T \qquad (35)$$

where $\boldsymbol{g}_n(k) = [g_{n1}, g_{n2}, \ldots, g_{nM}]$, for $k = 1, 2, \ldots, M$, with the individual g_{nk} given as

$$g_{nk} = \frac{A_n}{\sqrt{2\pi\sigma_n^{\,2}}} e^{\frac{-(k-\mu_n)^2}{2\sigma_n^{\,2}}} \qquad (36)$$

The values for A_n, σ_n and μ_n for each $\boldsymbol{g}_n$ vector are experimentally tweaked to create precise peaks (i.e., latencies) with progressively descending amplitudes at 100, 200, and 300 ms simulating the real P100, P200 and P300, respectively. By the same token, valleys at 75 and 145 ms are created to represent the N75 and N145, respectively. A generated VEP sample with realistically simulated amplitudes, showing precisely the N75, P100,

N145, P200 and P300 components are shown in Fig. 3(a) below.

The pre-stimulation EEG colored noise $\boldsymbol{e}(k)$ is generated using autoregressive (AR) model [12, 13, 14] given by the following equation.

$$\boldsymbol{e}(k) = 1.5084\boldsymbol{e}(k-1) - 0.1587\boldsymbol{e}(k-2) - 0.3109\boldsymbol{e}(k-3) - 0.0510\boldsymbol{e}(k-4) + \boldsymbol{u}(k) \quad (37)$$

where $\boldsymbol{u}(k)$ is the input driving noise of the AR filter and $\boldsymbol{e}(k)$ is the filter output. The artificial post-stimulation EEG noise $\boldsymbol{n}$ is generated by changing the variance of $\boldsymbol{e}$. Since noise is assumed to be additive, the artificially-corrupted VEP signal $\boldsymbol{y}$ is then produced by adding together $\boldsymbol{x}$ and $\boldsymbol{n}$.

As a preliminary illustration, Fig. 3 below shows, respectively, a sample of artificially generated VEP according to Eqs. (35) and (36), a noisy VEP at SNR = -10 dB, and extracted VEPs using both the GSA and TOC techniques.

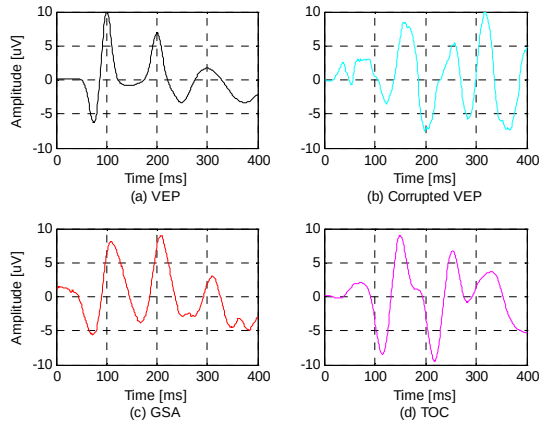

Fig. 3 (a) Clean VEP; (b) Noisy VEP with SNR = -10 dB; (c) Extracted VEP using GSA; (d) Extracted VEP using TOC.

From Fig. 3 above, it can be observed that GSA manages to extract and bring the P100, P200 and P300 peaks much closer to the their reference values (i.e., 100, 200 or 300 ms) compared to TOC. Further, to compare the performances of the two algorithms in statistical forms, the SNR was varied from 0 to -13 dB and the algorithms were run 500 times for each value. Failure rate and average errors are used in this paper as vital test tools in assessing the performance of the filters in single-trial estimation.

To measure failure rate, visual inspections were performed to judge whether or not the estimators' processed waveforms are acceptable. The three highest peaks within 100 ±10, 200 ±10 and 300 ±10 ms are considered as the wanted P100, P200 and P300 components. Any trial is noted as a failure with respect to a certain peak if the waveform fails to show clearly the pertinent peak within the stated ±10 ms tolerance. The failure rate for each algorithm with respect to a certain peak and SNR is expressed in terms of a percentage. It is calculated according to the following formula:

$$\text{failure rate} = \frac{\text{number of failures}}{N} \text{x } 100\% \quad (38)$$

where N is the number of runs (trials) per SNR which in this case equals to 500.

The average error in estimating P100 is obtained as follows:

$$\bar{\varepsilon}_{P100} = \frac{\left(\sum_{i=1}^{N} \left| \hat{t}_{P100}(i) - 100 \right| \right)}{N} \quad (39)$$

where $\hat{t}_{P100}(i)$ is the estimated latency (for each run) of the P100 in milliseconds. The average errors for P200 and P300 components can be calculated in the same way. The failure rates and average errors for the simulated data are shown in Table 1 below.

Table 1: The failure rate and average errors of GSA and TOC as a function of SNR.

SNR [dB]	Failure Rate [%]			Average error		
	Peak	GSA	TOC	Peak	GSA	TOC
-13	P100	9.3	71.3	P100	5.6	12.6
	P200	12.7	75.8	P200	6.3	14.1
	P300	23.1	74.2	P300	7.4	16.2
-11	P100	8.4	68.4	P100	4.6	10.7
	P200	11.6	74.8	P200	5.7	12
	P300	18.2	72.4	P300	5.8	14.3
-9	P100	8	69.6	P100	5	8.9
	P200	8.8	69.2	P200	4.9	11.2
	P300	20.2	74.2	P300	6.2	13.6
-7	P100	6.8	68.6	P100	4.5	7.4
	P200	7.2	71.2	P200	4.7	8.8
	P300	22.4	76.6	P300	6.9	12.8
-5	P100	3.1	69	P100	4.2	5.7
	P200	18.4	73	P200	4.5	7.3
	P300	61.4	72.4	P300	6.5	12.1
-3	P100	2.9	72.2	P100	4.1	5
	P200	2.4	72	P200	4.3	5.5
	P300	19.4	71	P300	6	11.3
0	P100	0.6	73	P100	3.7	4.1
	P200	0.4	70.8	P200	3.9	4.3
	P300	17.8	70.6	P300	6.5	9.8

From Table 1 it is clear that the proposed GSA algorithm outperforms TOC in terms of failure rates and accuracies over the considered range of SNRs. The GSA method shows performance that is relatively independent of SNR values. On the contrary, TOC's performance is poor. In general, both algorithms show better efficiencies in

estimating the latencies of P100's than they are with the other P200 and P300 peaks.

The strength of GSA is that it utilizes optimization and includes pre-stimulation EEG as one of its important parameters. As for TOC, it relies only on the observed (corrupted) VEP which comprises the clean VEP signal that is added to the post-stimulation EEG. In other words, TOC does not make use of the pre-stimulation EEG at all.

The TOC technique works on a basis that the encountered post-stimulation EEG resembles white or colored Gaussian noise. However, TOC performs well in handling white or colored noise whose spectrum does not directly overlap with that of the desired VEP signal.

To validate the performance of the two estimators, the next experiments will deal with real patient data. Nevertheless, the performance outcome and evidence collected in the simulated experiments above are the utmost crucial in proving the true capabilities of the filters as single-trial estimators; this is because the true forms of the individual VEPs from real patient data are not known *a priori*.

4.2 Real Patient Data

In this subsection, the accuracies of GSA and TOC as single-trial estimators of the P100 latencies, used in the objective assessment of the visual pathways from the retina to the visual cortex of the human brain, are tested. Real patient experiments were conducted at Selayang Hospital, Kuala Lumpur using RETIport32 equipment. The experiments were carried out on **normal** subjects without any neurological deficit or medication known to affect the EEG.

Subjects were asked to watch a checkerboard pattern (1^o full field), the stimulus being a checker reversal ($N = 50$ stimuli). Scalp recordings were made according to the International 10/20 System, with one eye closed at any given time. The active electrode was connected to the middle of the occipital (O1, O2) area while the reference electrode was attached to the middle of the forehead.

In this paper, we will show the results for artefact-free trials of **six** subjects taken from their left eyes only; for this purpose, each subject's left eye was left open while his/her right eye was shaded by an eye patch. Each trial was pre-filtered in the range 0.1 to 70 Hz and sampled accordingly, creating 512 data points within a 333 ms span.

Each subject underwent two separate recording sessions. In the first session, fifty trials for each subject were obtained and automatically averaged (using ensemble averaging) by the RETIport32 equipment to get the VEP signal and accordingly the latency of P100, which is the peak of interest of doctors at the Ophthalmology Department, Selayang Hospital.

Since averaging is a multi-trial technique, it is expected to produce good estimation of the VEP latency that can be used as a baseline for comparing the performances of GSA and TOC.

In the second session, 333 ms (machine dependent) of recording time was allocated to capture the brain activity just before a visual stimulation was applied to the subject. The recorded data for the entire 333 ms duration pertain to the pre-stimulus EEG signal which basically describes the brain background colored noise.

Then, the next 333 ms was used to record the post-stimulus waveform which comprises the VEP and post-EEG signals. These pre- and post-stimulation signals are required by the GSA algorithm.

As for TOC, there is no need for any pre-stimulus EEG signal; therefore, only the 333 ms of the post-stimuli waveform is considered for further processing.

The P100 latencies of six different subjects estimated by the single-trial GSA and TOC estimators, together with the corresponding P100 values approximated by the multi-trial ensemble averaging (EA) are shown in Figs. 4(a) through 4(f) below.

From Figs. 4(a) through 4(f), it can be stated that GSA outperforms TOC in estimating the latencies of the P100 components. The GSA method manages to extract the required P100 peaks; the latency values generated by GSA are closer to those generated by EA compared to those produced by TOC.

In brief, the simulated and real data experiments exhibit the capability of the subspace-based technique such as GSA in VEP latency estimation. Most importantly, the results of both experiments prove higher reliabilities (i.e., lower failure rate) and higher accuracies (lower average errors) of the proposed GSA algorithm over the third order correlation approach such as TOC.

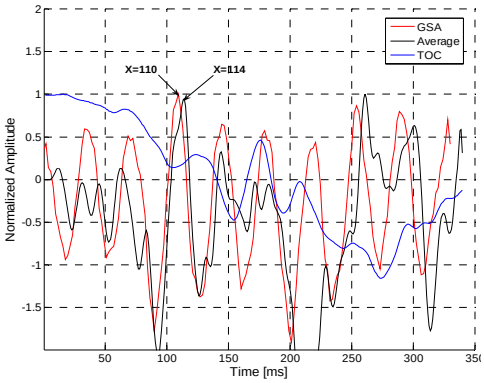

(a)

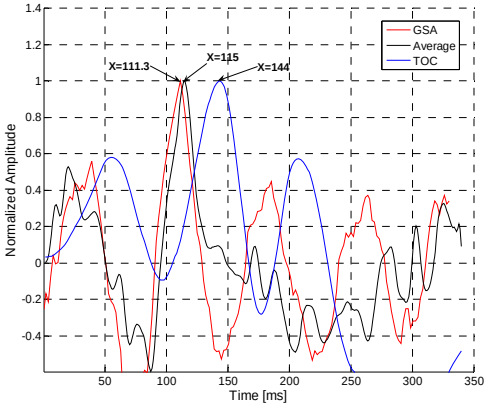

(b)

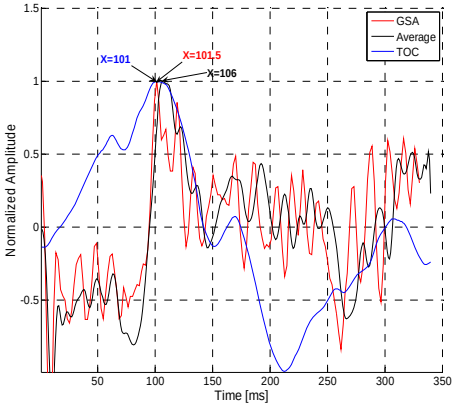

(c)

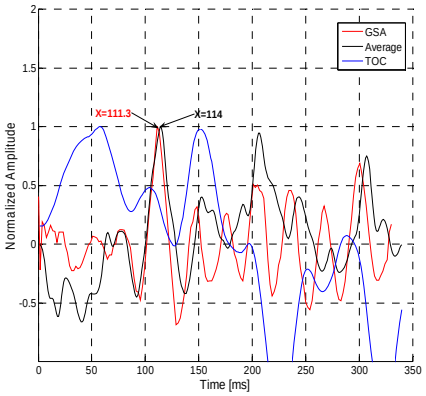

(d)

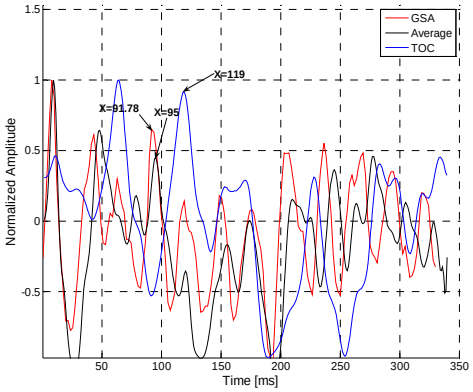

(e)

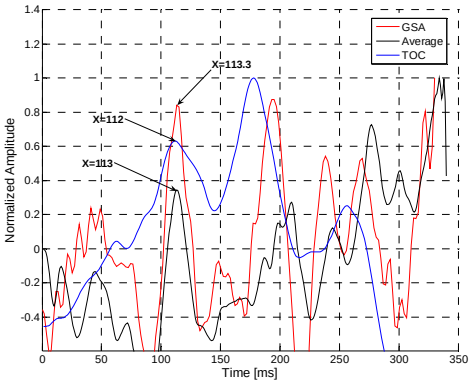

(f)

Fig. 4 The latency of P100 for six subjects estimated using the GSA and TOC, and 50-trials based EA techniques.

5. Conclusion

A signal subspace technique for extracting VEP signals degraded by colored EEG noise has been suggested and thoroughly tested. The algorithm which avoids an explicit pre-whitening stage utilizes an optimization procedure to develop an estimator which reduces a noise level below a certain threshold and maintains VEP distortion to a minimal value. As further enhancement, the proposed technique employs a generalized subspace scheme to simultaneously diagonalize both VEP signal and colored EEG noise correlation matrices.

The performance of the proposed GSA is compared with the TOC using simulated and real data. For simulated data, GSA shows better performance over TOC in detecting the latencies for P100, P200, and P300 peaks. Also, the results of the real patient experiments show better accuracy, less failure rate and closer results to the multi-trial ensemble averaging (EA) by GSA in comparison to TOC, in the P100 estimation. The performance reflects the capability of the single-trial GSA technique to replace the multi-trial EA technique in estimating VEP latencies, leading to the reduction in both recording time and user fatigue.

Acknowledgments

We would like to thank Dr. Tara Mary George and Mr. Mohd Zawawi Zakaria of the Ophthalmology Department, Selayang Hospital, Kuala Lumpur for acquiring the VEP data.

References

[1] L. Huszar, "Clinical Utility of Evoked Potential," eMedicine, April 18, 2006, retrieved May 5, 2006 from http://www.emedicine.com/neuro/topic69.htm.

[2] D. Regan, *Human brain electrophysiology: evoked potentials and evoked magnetic fields in science and medicine*, New York: Elsevier, 1989.

[3] G. Henning and P. Husar, "Statistical Detection of Visually Evoked Potentials," IEEE Engineering in Medicine and Biology, vol. 14, no. 4, pp. 386-390, July/August 1995.

[4] R. Q. Quiroga and H. Garcia, "Single-trial event related potentials with wavelet denoising," Clinical Neurophysiology, 114 (2003), pp. 376-390.

[5] P. Husar and G. Henning, "Bispectrum Analysis of Visually Evoked Potential," IEEE Engineering in Medicine and Biology, pp. 57-63, January/February 1997.

[6] H. O. Gulcur, M. Demirer and T. Demilrap, "An RBF Approach to Single Trial VEP Estimation," IEEE EMBS Conference, pp. 54-56, 1997.

[7] R. R. Gharieb and A. Cichocki, "Noise Reduction in Brain Evoked Potentials Based on Third-Order Correlations," IEEE Transactions on Biomedical Engineering, vol. 48, no. 5, pp. 501-512, May 2001.

[8] Y. Ephraim and H. L. Van Trees, "A Signal Subspace Approach for Speech Enhancement," IEEE Transaction on Speech and Audio Processing, vol. 3, no. 4, pp. 251-266, July 1995.

[9] B. C. Levy. *Principles of Signal Detection and Parameter Estimation*, Springer Science+Business Media, LLC, New York, 2008.

[10] J. T. Scheick, *Linear Algebra with Applications*, McGraw-Hill, New York, 1997.

[11] S. Andrews, R. Palaniappan and N. Kamel, "Extracting Single Trial Visual Evoked Potentials using Selective Eigen-Rate Principal Components", World Enformatika Society Transactions on Engineering, Computing and Technology, vol. 7, pp. 330-333, August 2005.

[12] X. H. Yu, Z. Y. He and Y. S. Zhang, "Time-Varying Adaptive Filters for Evoked Potential Estimation," IEEE Transactions on Biomedical Engineering, vol. 41, no. 11, pp. 1062-1071, November 1994.

[13] A. Cichocki, R. R. Gharieb and T. Hoya, "Efficient Extraction of Evoked Potentials by Combination of Wiener Filtering and Subspace Methods", IEEE Transactions on Biomedical Engineering, pp. 3117-3120, 2001.

[14] X. Xiong and Y. Chen, "Extracting ERP by Combination of Subspace Method and Lift Wavelet Transform," in *Proc. 27th Annual Conference of IEEE Engineering in Medicine and Biology Society (IEEE-EMBS 2005)*, Shanghai, China, September 1-4, 2005, pp. 5938-5941.

Mohd Zuki Yusoff was born in 1966. He received his BSc in Electrical Engineering in 1988 from Syracuse University, USA, and MSc in Communications, Networks & Software in 2001 from Surrey University, England. He received his PhD in Electrical & Electronic Engineering from Universiti Teknologi Petronas, Malaysia in 2009. He is currently a lecturer at Universiti Teknologi Petronas. His research interests include signal processing and embedded systems.

Nidal Kamel was born in 1961. He received his MSc in Hydroacoustics systems in 1989 and PhD degree in telecommunication and statistical signal processing from the Technical University of Gdansk, Poland, in 1993. His research is focused on signal processing, parameter estimation and noise reduction. He is currently an Associate Professor at Universiti Teknologi Petronas, Malaysia. He is senior member of IEEE.